Pergamon

Geochimica et Cosmochimica Acta, Vol. 67, No. 14, pp. 2543–2550, 2003

0016-7037/03 $30.00 + .00

doi:10.1016/S0016-7037(02)01350-9

Uranium (VI) sorption on colloidal magnetite under anoxic environment: Experimental study and surface complexation modelling

TIZIANA MISSANA,* MIGUEL GARCÍA-GUTIÉRREZ, and VICTOR FERNÁNDEZ
CIEMAT, Departamento de Impacto Ambiental de la Energía, Avenida Complutense, 22, 28040 Madrid, Spain

(*Received July* 29, 2002; *accepted in revised form November* 11, 2002)

Abstract—Magnetite is one of the most important end member of iron corrosion products under a reducing environment; therefore, it may be one of the first products interacting with radionuclides in a radioactive waste disposal after the canister failure.

Nanocrystalline magnetite was synthetised in the laboratory and its main physico-chemical properties (microstructure, surface area, surface charge) were analysed. The stability of the oxide was also investigated under the experimental conditions used in sorption studies. The sorption behaviour of U^{VI} onto magnetite was analysed under O_2- and CO_2-free conditions in a wide range of pH, ionic strengths and radionuclide concentrations.

The uranyl binding to magnetite is characterised by a sorption edge between pH 4 and 5.5, and sorption was found to be independent on the electrolyte concentration, which indicates the formation of inner sphere complexes. The sorption isotherms showed a linear behaviour up to the saturation of the sorption sites with a Langmuir-type behaviour.

One of the aims of this work was to find the simplest model capable to reproduce the experimental data. Sorption data were fitted using a classical approximation (diffuse double layer model), considering only one type of surface site and evaluating two different options: the first one involving two different monodentate complexes, and the second one a single binuclear bidentate complex. A highly satisfactory fit of the experimental data was obtained by both approaches in the range of the experimental conditions investigated.

1. INTRODUCTION

One of the options for the final disposal of the high level radioactive waste is the deep geological repository. The aim of these disposals is to ensure that the possible release of radionuclides will be delayed until their radiological impact is negligible (Chapman and McKinley, 1987). In the repository, the radioactive waste is placed in metallic containers, which represent the first physical barrier to radionuclide migration. The release of radionuclides can occur, a few hundred years after the emplacement, originated by the canister failure due to iron corrosion (Hoch et al., 1997). Their migration behaviour can be substantially affected by the presence of corrosion products: iron corrosion can generate a reducing environment, thus, keeping many radionuclides in a less mobile form and, furthermore, these products may act as a sorbing layer and favour radionuclide immobilisation.

One of the corrosion products of steel in oxygen-poor environments is the green-rust, that is, a hydroxide containing both Fe^{II} and Fe^{III} (Cornell and Schwertmann, 1996). Green rusts are generally metastable and they tend to evolve to more stable crystalline phases. It has been reported that the main stable end member of oxides transformations in moderate to strong reducing environments and neutral-alkaline conditions is magnetite (Cornell and Schwertmann, 1996). In addition, magnetite has been observed in previous experimental studies on steel corrosion in conditions simulating the repository (Gdowski and Estill, 1996; Grambow et al., 1996; Inagaki et al., 1996). Therefore, the study of the interactions of radionuclides with magnetite should be evaluated to predict their migration within these systems.

Uranium is a very important element in the context of radioactive disposals because it is the major waste component and, together with its daughter products, can significantly contribute to the radiological impact. In particular, the study of the U^{VI}/magnetite system is of interest for the understanding of the sorption/redox processes occurring to uranium after the oxidative dissolution of the spent fuel.

Batch sorption studies are essential to understand the uptake mechanisms of radionuclides into a mineral phase. Over the last 20 yr, numerous papers have dealt with the study of the interaction of radionuclides, and in particular uranium, with Fe^{III} oxy-hydroxides, but much less is known about their interactions with oxides containing Fe^{II}. In addition, the surface charge properties of Fe^{III} oxides have been intensively studied and this allowed a wide application of surface complexation models for the interpretation of adsorption processes (Hsi and Langmuir, 1985; Waite et al., 1994). On the other hand, both surface characterisation and sorption studies are considerably more limited in the case of magnetite.

Previous studies on the sorption of U^{VI} onto magnetite exist: for example, El-Aamrani et al. (2000) studied the effects of carbonate on the U^{VI} uptake onto magnetite at a single pH and ionic strength; Sagert et al. (1989), performed U^{VI} sorption isotherms in presence of bicarbonates in a pH range between 7 and 9 onto a "magnetite" with a very low Fe^{II}/Fe^{III} ratio (0.08) and in aerobic conditions; Venkataramani and Gupta (1991) studied the effects of anions on the sorption of uranyl in magnetite at a fixed ionic strength and uranyl concentration.

* Author to whom correspondence should be addressed (tiziana.missana@ciemat.es).

However, to our knowledge, the sorption behaviour of U^{VI} onto magnetite under anoxic environment has not been studied yet in a range of experimental conditions wide enough to apply reliable surface complexation modelling.

The aim of this work is to study the sorption of U^{VI} onto magnetite in CO_2- and O_2-free conditions and to interpret the sorption data using the simplest surface complexation model that is capable to fit them satisfactorily. The use of simple models would greatly facilitate their application in the performance assessment calculation of radioactive waste disposals.

Adsorption edges (from pH 3–10) and sorption isotherms were carried out at different ionic strengths (from $1 \cdot 10^{-3}$ to $2 \cdot 10^{-1}$ mol/L), to obtain sorption values in a wide range of experimental conditions. The iron oxide used in this work was synthesised in laboratory and characterised by means of transmission electron microscopy (TEM), X-ray diffraction (XRD) and X-ray photoelectron spectroscopy (XPS). The basic parameters needed for the application of surface complexation modelling (surface sites density, surface charge and surface area) were also experimentally determined. Before the sorption studies, the stability of the magnetite in suspensions under different experimental conditions was also analysed.

The results showed that the uranyl binding with the magnetite surface involves inner sphere complexes. Two different simple modelling approaches gave a very good agreement between simulation and sorption data over the entire range of experimental conditions considered.

2. MATERIALS AND METHODS

All the reagents were of analytical grade and they were used without further purification. The desionised water (MilliQ-Milliρ system), used to prepare the electrolytes and suspensions, was bubbled with N_2 and boiled for at least 15 min, to minimise CO_2 contamination, before its storage in an anoxic glove box. The atmosphere in the anoxic glove box was CO_2-free nitrogen ($O_2 < 1$ ppm). All the experiments described below were run at room temperature.

2.1. Oxide Preparation and Characterisation

Different batches of magnetite were prepared using a synthesis method described in (Schwertmann and Cornell, 1996). Five hundred sixty milliliters of a solution of 0.3 mol/L $FeSO_4$ were heated to 90°C and 240 mL of a solution 3.33 mol/L in KOH and 0.27 mol/L in KNO_3 were added very slowly. The suspension was maintained at 90°C for 1 h with continuous stirring. All these processes were carried out flushing N_2. Hydrazine was added to the suspension, to prevent the formation of unwanted ferric oxides during the nucleation stage and to improve the quality of the magnetite sample. After the synthesis process, a dark black solid was obtained, that was decanted and introduced in dialysis bags for the washing step. Extensive washing was needed to remove all the salts from the solid and, to avoid the oxidation of the iron oxide during this step, the procedure was carried out in an anoxic glove box. The dialysis bags were placed in a 1-L container filled with deionised and degassed water, that was periodically changed until its conductivity was stable and <10 μS/cm. This assured the removal of any salt from the oxide. The excess of water was then eliminated and the solid dried under N_2 atmosphere. The solid samples were finally stored in the anoxic glove box.

The microstructure of the samples was analysed by transmission electron microscopy (TEM) and selected area diffraction patterns (SADP) using a Philips Electron Microscope at 80 kV. TEM samples were prepared by depositing a drop of the suspension onto a carbon-coated Cu grid. XRD analysis was performed with a Philips XPert-MPD and surface area was determined with the BET method using a Micromeritics Flowsorb II 2300 apparatus. XPS analysis was performed with a Perkin-Elmer PHI 5400 spectrometer equipped with a Mg Kα* excitation source ($h\nu = 1253.6$ eV) and a beam size of 1 mm diameter. Typical operation conditions were: X-ray gun, 15 kV, 20 mA; pressure in the sample chamber $\approx 10^{-9}$ torr; pass energy 89.5 eV for general spectra (0–1100 eV) and 35.75 eV for high-resolution spectra. To take into account the charging effects on the measured binding energies, these energies have been determined by referencing to the adventitious C 1s peak at 284.8 eV.

2.2. Preparation of the Suspensions; Stability of the Oxide and Surface Acidity

The iron oxide suspensions were prepared in the anoxic glove box by adding 2 g/L of the solid powder to the electrolyte ($NaClO_4$) at different ionic strengths. After the addition of the solid, the suspensions were placed in an ultrasonic bath for 1 h and then both solid and solution were allowed to equilibrate at least for 1 d.

The stability of the iron oxide in the electrolyte solutions was studied by evaluating its degree of dissolution at different pH and contact times. The pH measurements were carried out with a Metrohlm glass electrode calibrated with three buffer solutions (pH 4, 7 and 10) before and after the experiment. Aliquots of 30 mL of the suspensions were prepared at different pH (3, 5, 7, 9.5 and 11) and were introduced in ultracentrifuge tubes. After a certain amount of time (1 d, 1 week, 2 weeks, 1 month and 3 months), these aliquots were ultra-centrifuged (504,000 g, 1 h) and the total iron content in the supernatant was analysed by plasma spectrometry.

Potentiometric acid/base titrations were used to determine the surface acidity constants. To take into account the possible effects of the ionic strength on the electrode readings, an additional electrode calibration was carried out before the titrations experiments using samples of known hydrogen ion concentration in $NaClO_4$ at three different ionic strengths ($1 \cdot 10^{-1}$, $1 \cdot 10^{-2}$, $1 \cdot 10^{-3}$ mol/L). The magnetite/$NaClO_4$ suspensions (2 g/L) were titrated in polyethylene vessels and in the anoxic glove box to exclude CO_2 from the system.

The acid and base used to change the pH were NaOH and HCl 0.1 mol/L, and the acid/base additions were made about every 2 to 3 min (fast titrations). For each suspension, a first titration was carried out starting from the initial pH to pH 3 and then titrating the sample back to pH 10. A second titration was carried out from the initial pH to pH 10 and then titrating back to pH 3. No significant hysteresis between acid and base titration curves was observed using this "fast titration" procedure.

2.3. Sorption Experiments: Sorption Edges and Isotherms

All the sorption experiments were carried out in the anoxic glove box under N_2 atmosphere. Suspensions of magnetite were prepared, as previously described, at different ionic strengths ($I = 2 \cdot 10^{-1}$, $1 \cdot 10^{-1}$, $1 \cdot 10^{-2}$ and $1 \cdot 10^{-3}$ mol/L). Sorption edges were carried out changing the pH of these suspensions from pH ~3 to 10.

Three different aliquots of the suspension, at the selected pH, were introduced in 12.4 mL ultracentrifuge tubes and $^{233}U^{VI}$ was added to a final concentration of $4.4 \cdot 10^{-7}$ mol/L. After the radionuclide addition, the tubes were sealed and maintained in continuous stirring for 4 h or 1 d, and afterwards they were ultra-centrifuged (645,000 g, 30 min). This centrifugation ensured the complete sedimentation of colloids. After the solid separation, two aliquots of the supernatant from each tube were extracted for the analysis of the final activity. The activity in the supernatant was measured by liquid scintillation with a Packard counter. The detection limit for uranium is $\sim 1 \cdot 10^{-9}$ mol/L. The rest of the solution was used to check the pH.

Sorption isotherms were carried out at a fixed pH (pH = 7) and varying the U^{VI} concentration from $5 \cdot 10^{-9}$ to $1 \cdot 10^{-4}$ mol/L, approximately. The highest uranium concentrations were achieved by also adding uranyl nitrate ($UO_2(NO_3)_2 \cdot 6H_2O$, Mercks). The separation and counting procedure was the same than that used for sorption edges.

2.4. Modelling

The modelling of titration and sorption experiment was carried out with the classical diffuse double layer (DDL) model (Stumm et al., 1970; Huang and Stumm, 1973; Dzombak and Morel, 1990). In this model, the oxide water/interface is described as two layers of charge.

The first layer of charge is located at the oxide surface and produced by the specifically adsorbed ions. A diffuse layer of counter ions, that balance the surface charge, is located in the solution near the solid. The distribution of the ions in the diffuse layer follows the Gouy-Chapman equation.

The reactions at the surface of the oxide mainly involve the amphoteric surface functional groups (SOH). The pH-dependent charge is determined by the following protonation/deprotonation reactions:

$$SOH_2^+ \Leftrightarrow SOH + H^+ \qquad K_{a1} \tag{1}$$

$$SOH \Leftrightarrow SO^- + H^+ \qquad K_{a2} \tag{2}$$

where SOH^{2+}, SOH and SO^- represent the positively charged, neutral and negatively charged surface sites, respectively, and K_{a1} and K_{a2} are the intrinsic equilibrium acidity constants. The mass law equations corresponding to the reactions Eqn. 1 and 2 are

$$K_{a1} = \frac{(SOH)\{H^+\}}{(SOH_2^+)} \exp\left(-\frac{F\psi}{RT}\right) \tag{3}$$

$$K_{a2} = \frac{(SO^-)\{H^+\}}{(SOH)} \exp\left(-\frac{F\psi}{RT}\right) \tag{4}$$

where { } represents the ion activity and () the ion concentrations. Since the activity coefficients for all the surface species are assumed to be equal the activity of these species can be substituted by their concentration (). The exponential represents the coulombic term that accounts for the electrostatic effects (Dzombak and Morel, 1990). Ψ represents the surface potential, R the molar gas constant, T the absolute temperature (K) and F the Faraday constant.

Specific adsorption of cations at the surface functional groups can be described with reactions of the following type:

$$SOH + M^{z+} \Leftrightarrow SOM^{z-1} + H^+ \qquad K_c \tag{5}$$

$$\text{with } K_c = \frac{(SOM^{z-1})\{H^+\}}{(SOH)\{M^{z+}\}} \exp\left(-\frac{(z-1)F\psi}{RT}\right) \tag{6}$$

for a monodentate binding or

$$2SOH + M^{z+} \Leftrightarrow (SOH)_2M^{z-2} + 2H^+ \qquad \beta_c \tag{7}$$

$$\text{with } \beta_c = \frac{[(SOH)_2M^{z-2}]\{H^+\}^2}{(SOH)^2\{M^{z+}\}} \exp\left(-\frac{(z-2)F\psi}{RT}\right) \tag{8}$$

for bidentate binuclear binding, where the SOH groups interacts independently with the metal ion.

The calculations were done with the CHESS code v 2.4 (van der Lee and De Windt, 1999) and the fits of the experimental curves were obtained with a trial and error procedure. The best fit was find trying to minimise the χ^2 function. The χ^2 is defined as:

$$\chi^2 = \frac{1}{\nu}\sum_1^N \frac{(y_f - y_i)^2}{\sigma_i^2} \tag{9}$$

where y_f is the model (the fit) estimate, y_i is the actual observation, and σ_i in the denominator is the uncertainty in the individual measurement (y_i) and ν represents the degrees of freedom ($\nu = N - p - 1$ where N is the number of observations, and p is the number of coefficients or parameters used in the regression fit).

3. RESULTS AND DISCUSSION

3.1. Characterisation of the Oxide

Figure 1 shows the XRD (Fig. 1a) and the XPS (Fig. 1b) spectra of the solid material synthesised as described in the experimental section. The peaks of the XRD spectrum of the solid fit very well with those expected for magnetite (Fe_3O_4) and another different mineral phase could not be detected. However, since the XRD spectrum of magnetite

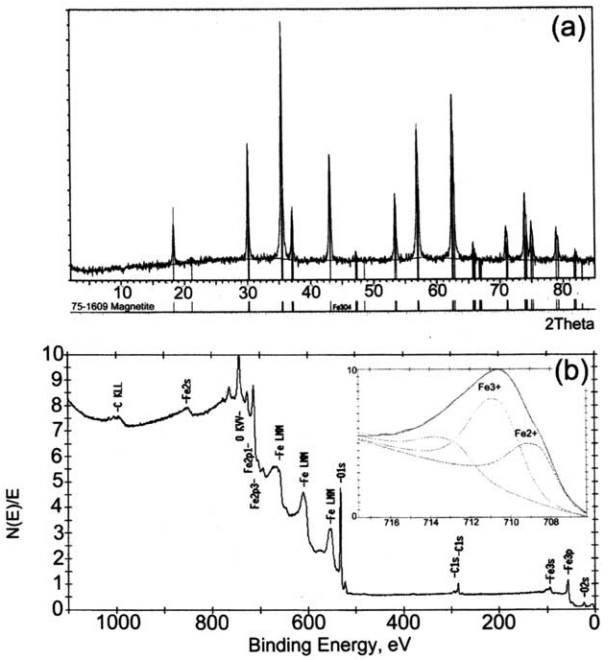

Fig. 1. (a) X-ray diffraction and (b) XPS spectrum of the magnetite used in this work. In the inset of (b) a detail of the deconvolution of the Fe 2p3/2 peak is shown.

($Fe^{II}OFe^{III}_2O_3$) and that of its isostructural form γ-Fe_2O_3 (maghemite), in which all or most of the Fe is in trivalent state, are actually difficult to distinguish, XPS measurements are needed to verify the iron oxidation state in the solid. The XPS analysis confirmed that the oxide was magnetite with a Fe^{II}/Fe^{III} ratio ranging from 0.3 to 0.67, with a mean value only slightly lower (0.45) than the expected stoichiometric one (0.5). A detail of the $Fe2p_{3/2}$ peak is shown in the inset of Figure 1b. This peak shows a binding energy with an Fe^{II} component clearly visible.

The microstructural characteristics of magnetite strongly depend on the methodology selected for its synthesis (Regazzoni et al., 1981) and, particularly, on the pH and ionic strength of the precipitation medium (Vayssieres et al., 1998). Figure 2 shows a TEM picture of the magnetite sample used in this work. It is formed by small crystals (whose sizes range from 50–200 nm) showing well-defined edges (cubic or octahedral shapes). The microstructure observed in different experimental batches was always very similar. The main lattice spacings, experimentally measured in the selected area diffraction pattern included in Figure 2 (4.855, 2.967, 2.543 and 2.094 Å), correspond very well to the *hkl* values ((111), (220), (311), (400)) reported for polycrystalline magnetite.

The measured BET surface area of this nanocrystalline magnetite was 8.5 m^2/g. The surface area of magnetite depends on the microstructure of the sample and on its grain size (Regazzoni et al., 1981) and, obviously, on the method used for the determination. Since magnetite is a no porous material (Cornell and Schwertmann, 1996), very high values of surface area implies the presence of impurities of high specific area. The value obtained in this work is in agreement with previously

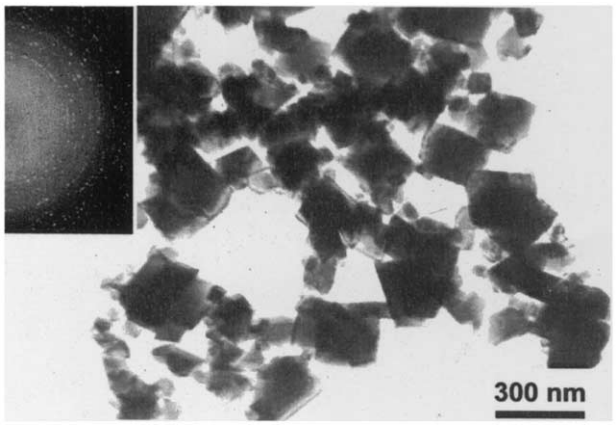

Fig. 2. Transmission electron microscope image of the magnetite used in this work. The inset in the figure shows the selected area in diffraction pattern, which corresponds approximately to the area of the picture.

reported values by different authors in samples with similar microstructure (Blesa et al., 1984; Shen et al., 1999).

3.2. Stability of the Oxide

Figure 3 shows the results of stability experiments performed on magnetite (2 g/L, $I = 0.1$ mol/L). The degree of dissolution of the oxide was evaluated at different pH and contact times. The total iron, experimentally determined in the supernatant solution, is plotted in Figure 3 and the dotted line represents the theoretical dissolution curve calculated with the Chess code. Magnetite is very stable in the neutral and basic pH range where, in fact, the total iron measured in solution was always near or below the detection limit (0.02 ppm), but tends to dissolve at acid pH (pH < 4). This is not surprising since Fe^{II} oxides are reported to be more soluble than Fe^{III} oxides and magnetite is more soluble than $Fe(OH)_2$ (Cornell and Schwertmann, 1996). Since the experimental results show that the magnetite dissolution is a kinetically controlled process, it can be concluded that short experiments or experiments in neutral or alkaline conditions would not be influenced by the oxide dissolution. However, in larger time scale experiments, and above all at acidic pH, the dissolution process must be taken into account.

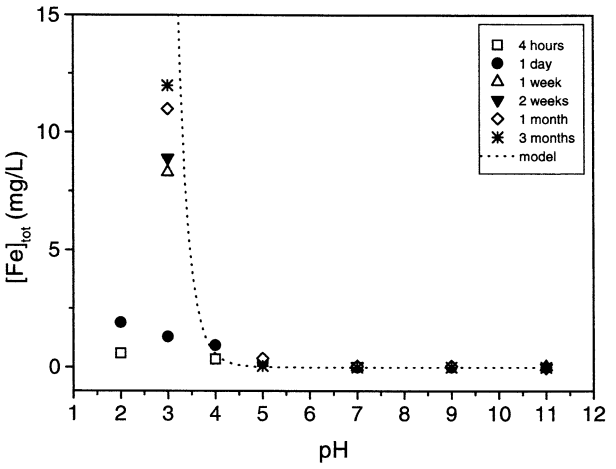

Fig. 3. Total iron concentration measured after different magnetite/solution contact times and at different pH.

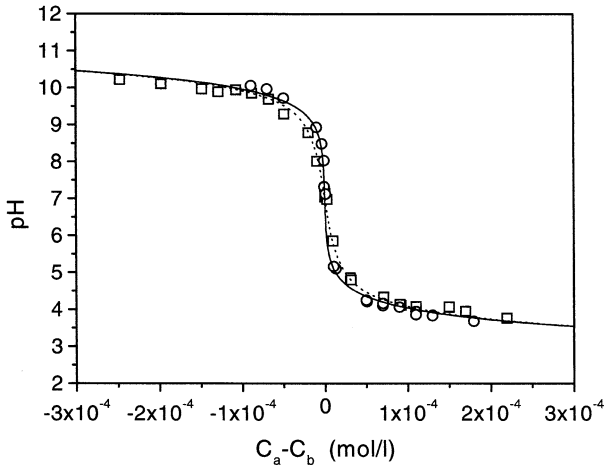

Fig. 4. Titration curves for magnetite suspension (2 g/L) at two different ionic strengths: (□) $I = 0.1$ mol/L and (○) $I = 1 \cdot 10^{-3}$ mol/L. The continuous lines correspond to the fit obtained with the DDL model and the parameters of Table 1. (. . .) $I = 0.1$ mol/L and (–) $I = 1 \cdot 10^{-3}$ mol/L.

3.3. Titration Experiments

Fast titrations (the addition of the acid/base was performed each 2 min approximately) have been preferred to batch experiments (Shultess and Sparks, 1986) to minimise the possible effects due to magnetite dissolution. Figure 4 shows the titration curves of magnetite obtained at the ionic strengths of $1 \cdot 10^{-1}$ and $1 \cdot 10^{-3}$ mol/L. The curves have a crossing point at pH $\sim$ 7. If H^+ is assumed to be the only specifically sorbing ion, the proton surface charge density (σ) is given by

$$\sigma = \left(\frac{F}{AS}\right)[(SOH_2^+) - (SO^-)] \text{in C/m}^2 \qquad (10)$$

or

$$\sigma = F(\Gamma_H - \Gamma_{OH})$$

where Γ_H and Γ_{OH} are the experimental sorption densities expressed in mol/m^2, F is the Faraday constant (96.485 C/mol), A the specific surface area (m^2/g) and S the solid concentration (g/L). The net consumption of H^+ or OH^- can be calculated by

$$\Gamma_H - \Gamma_{OH} = (1/AS)[C_A - C_B - (H^+) + (OH^-)] \qquad (11)$$

where C_A is the molar concentration of the acid added and C_B of the added base.

The logarithm of intrinsic acidity constant determined from the fit of the titration curves with the DDL model (Eqn. 1 and 2) are 5.1 and -9.1, respectively, with a pH_{PZC} of 7.1. (Table 1). The surface site density value used in the fit is $\sim 1 \cdot 10^{-4}$ mol/L (3.53 sites/nm^2) and the value was fixed during the

Table 1. Parameters used to model titration and sorption curves.

BET: 8.5 m^2/g		
SOH density: 3.54 sites/nm^2		
pH_{PZC}: 7.1		
	Surface acidity	
Specie	Composition	Log K
SO^-	SOH, $-H^+$	–9.1
SOH_2^+	SOH, $+H^+$	5.1
	Surface complexation model 1	
Specie	Composition	Log K
$SOUO_2+$	SOH, $-H^+$, $1UO_2^{2+}$	–0.10
$SOUO_2OH$	SOH, $-2H^+$, $1UO_2^{2+}$, $1H_2O$	–5.40
	Surface complexation model 2	
Specie	Composition	Log K
$(SO)_2UO_2$	2SOH, $-2H^+$, $1UO_2^{2+}$	–1.32

estimation of the acidity constants. The fits of titration curves are included in Figure 4 as lines.

The point of zero charge values, found in the literature for magnetite, are quite scattered. One reason for this is the difficulty to perform colloid chemical studies on aqueous magnetite dispersions, since magnetic forces may overlap the double layer interactions (Regazzoni et al., 1981). In addition, soluble and redox sensitive minerals pose substantial problems for the study of their surface charge. In most of the literature data, however, the pH_{PZC} is located in the near neutral pH region, in agreement with our result (Tewari and McLean, 1972; Marmier et al., 1999; Blesa et al., 1984). Furthermore, Wesoloski et al. (2000) estimated a point of zero charge for magnetite between 6.5 and 7 with the MUSIC model.

3.4. Sorption Edges and Sorption Isotherm

The contact time selected to study the sorption behaviour was <1 d (typically 4 h) to minimise possible solid dissolution and redox effects as well. In fact, few hours are enough to establish the sorption equilibrium as shown in a previous work (Missana et al., 2003). Furthermore, it was shown that, in O_2- and CO_2-free conditions similar to those used in these experiments, the Eh of equilibrium between the $NaClO_4$ electrolyte and magnetite was ~50 to 100 mV and that the kinetics of the attainment of this equilibrium was significantly slower than the sorption one (weeks). It is important to remark that within this Eh range, above all at acidic pH, the reduction of dissolved uranium is thermodynamically feasible, as well as the subsequent precipitation of U^{IV} solids. The reduction/precipitation of uranium in the solution would bias the sorption results and their modelling, therefore it has to be avoided.

Figure 5 shows the sorption edges of uranium onto magnetite obtained at different ionic strengths (from $1 \cdot 10^{-3}$ to $2 \cdot 10^{-1}$ mol/L), and different contact times (4 h, 1 d and 3 months). As can be seen, sorption increases from 0% at pH 3.5 to ~90% of the total uranium at pH 6. The pH corresponding to 50% of sorption is ~5. A non-negligible decrease in the sorption is observed at pH > 9, where the experimental data are also more scattered. Since a great care was taken to exclude CO_2 from the system, before and during the sorption experiments, it is not likely that this decrease could be attributed to CO_2 contamination.

Another fact to be remarked is that sorption does not depend

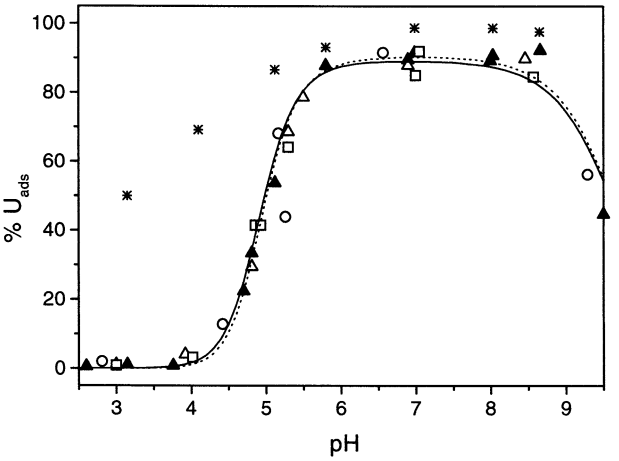

Fig. 5. Sorption edge at different ionic strengths: (▲) $I = 0.1$ mol/L, 1 d; (△) $I = 0.1$ mol/L, 4 h; (*) $I = 0.1$ mol/L, 3 months. (□) $I = 0.2$ mol/L, 4 h; (○) $I = 1 \cdot 10^{-3}$ mol/L, 4 h. The lines correspond to the modelling of the experimental data at $I = 0.1$ mol/L: (- - -) Model 1 and (—) Model 2. Solid to liquid ratio 2 g/L and [U] = $4.4 \cdot 10^{-7}$ mol/L.

significantly on the electrolyte concentration, within the experimental error. This fact suggests that inner sphere complexes are formed, as already reported for uranyl sorption on other iron oxides (Waite et al., 1994). The apparent independence of sorption on the ionic strength might be also due to weak electrostatic effects.

Finally it is worth noticing that no significant variation is observed between data collected after 4 h of contact time and those collected after 1 d ($I = 1 \cdot 10^{-1}$ mol/L). This confirms that the sorption equilibrium is reached within a few hours, as expected for cation sorption onto iron oxides oxides (Waite et al., 1994; Cornell and Schwertmann, 1996). Quite different sorption edges are obtained if the contact time between solution and magnetite is significantly greater. The data obtained after 3 months of contact time are also shown in Figure 5. Experimentally, a progressive disappearance of uranium from the liquid phase is observed, which leads to an apparent increase in sorption. Actually, as mentioned before, this behaviour can be explained considering the reduction/precipitation of uranyl in presence of magnetite (Missana et al., 2003).

Figure 6 shows the uranium sorption isotherm obtained at the ionic strength of $I = 1 \cdot 10^{-1}$ mol/L and pH 7. The results are expressed as the logarithm of the dissolved uranium concentration at the equilibrium (U_{eq}) in mol vs. the logarithm of the concentration of the adsorbed uranium (U_{ads}) in moles per gram. A region with linear sorption (slope of the isotherm ≈ 1) can be observed over a range of 4 orders of magnitude. The saturation starts when the U equilibrium concentration in solution is $>1 \cdot 10^{-6}$.

3.5. Modelling

One of the main aims of the present work is to fit the experimental data with the simplest model capable to reproduce them. As discussed above, the titration experiments were well simulated by supposing only one type of sorption sites. Furthermore, the isotherm curve, does not indicate the existence of

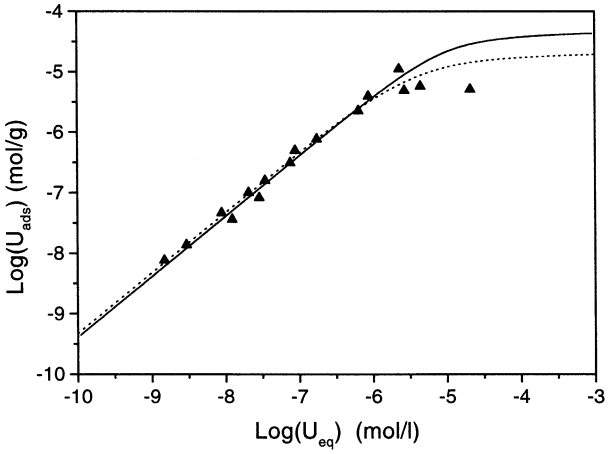

Fig. 6. Sorption isotherm at pH 7 and ionic strength $I = 0.1$ mol/L. The continuous line represents the fit of the data with Model 1 and the dotted one represents the fit of the data with Model 2.

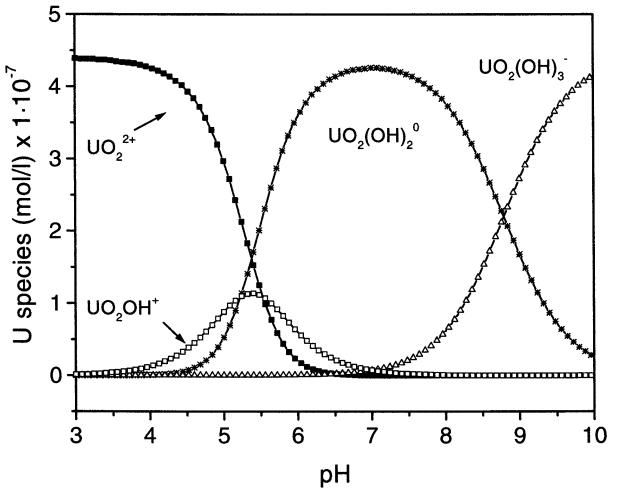

Fig. 7. Aqueous speciation of uranium with the thermodynamic data of Table 2. $I = 0.1$ mol/L and [U] = $4.4 \cdot 10^{-7}$ mol/L. Only major species are shown.

more than one sorption site. For sake of simplicity, the diffuse double layer model was therefore applied considering only one type of sorption sites (SOH). All the parameters needed for the modelling (surface area, sorption site density and acidity constants) were determined, thus, the only additional fitting parameters are the surface complexation constants.

It is generally accepted that the charged dominant aqueous species are those that most likely are involved in the formation of surface complexes. Since the U^{VI} aqueous speciation is complex, different complexes can be postulated and a unique modelling approach does not exist. The speciation as a function of the pH for uranium concentration of $4.4 \cdot 10^{-7}$ mol/L and ionic strength $1 \cdot 10^{-1}$ mol/L was calculated, supposing a zero partial pressure of CO_2 and using the sets of constants of Grenthe (1992) included in the EQ3/6 data base of the CHESS code. These species and their constants are summarised in Table 2. Some authors argue that the log K values of Table 2 indicated with * and ** should be substituted with ≤ -12 (Silva, 1992) and -20 (Sandino and Bruno, 1992), respectively. The discussion of this point is not an objective of the present work. Nevertheless, the comparison of modelling results obtained with the two sets of solubility constants for the sorption of uranyl on iron oxides can be found elsewhere (Missana et al., 2002).

Table 2. U(VI) aqueous phase reactions and stability constants from Grenthe et al. (1992).

Specie	Composition	Log K
UO_2OH^+	$-1H^+$, $1H_2O$, $1UO_2^{2+}$	–5.2
$UO_2(OH)_2^0$	$-2H^+$, $1H_2O$, $2UO_2^{2+}$	–10.3 (*)
$UO_2(OH)_3^-$	$-3H^+$, $3H_2O$, $1UO_2^{2+}$	–19.2 (**)
$UO_2(OH)_4^{2-}$	$-4H^+$, $4H_2O$, $1UO_2^{2+}$	–33.1
$(UO_2)_2(OH)^{3+}$	$-1H^+$, $1H_2O$, $2UO_2^{2+}$	–2.7
$(UO_2)_2(OH)_2^{2+}$	$-2H^+$, $2H_2O$, $2UO_2^{2+}$	–5.6
$(UO_2)_3(OH)_4^{2+}$	$-4H^+$, $3H_2O$, $4UO_2^{2+}$	–11.9
$(UO_2)_3(OH)_5^+$	$-5H^+$, $5H_2O$, $3UO_2^{2+}$	–15.6
$(UO_2)_3(OH)_7^-$	$-7H^+$, $7H_2O$, $3UO_2^{2+}$	–31.0
$(UO_2)_4(OH)_7^+$	$-7H^+$, $7H_2O$, $4UO_2^{2+}$	–21.9

The calculated aqueous speciation with the data of Table 2 is shown in Figure 7. The dominant species at pH < 5, a region where most of the adsorption process takes place, are UO_2^{2+} and UO_2OH^+. At pH between 5.5 and 8.5, $UO_2(OH)_2^0$ becomes the major dissolved species, whereas at higher pH the negatively charged $UO_2(OH)_3^-$ predominates. Therefore, as a first tentative modelling the two major species UO_2^{2+} and UO_2OH^+, were supposed to react with the iron oxide surface site, SOH, forming monodentate complexes, with K_c^1 and K_c^2 as surface complexation constant with the following reactions (Model 1):

$$SOH + UO_2^{2+} \Leftrightarrow SOUO_2^+ + H^+ \qquad K_c^1$$

$$SOH + UO_2OH^+ \Leftrightarrow SOUO_2OH + H^+ \qquad K_c^2$$

The sorption edges experimental data were plotted in Figure 8 expressed as the logarithm of the distribution coefficient (*Kd*) defined as follows

$$Kd = \frac{V}{m}\left(\frac{U_{ads}}{U_{eq}}\right)$$

where $(V/m)^{-1}$ is the solid to liquid ratio in g/mL and U_{ads} and U_{eq} are the concentration of adsorbed uranium and the dissolved uranium at equilibrium, respectively. This representation of the experimental data is very useful, because when sorption is near to saturation, the variations are better detected and it facilitates the fitting procedures.

The parameters used to fit the experimental curves with Model 1 are summarised in Table 1 with the reactions and their respective constants. The theoretical curves of uranium sorption onto magnetite calculated with the above-mentioned parameters for the three ionic strengths are shown superimposed to the experimental points in Figure 8a (sorption edges) and Figure 6 (sorption isotherm, continuous line).

This model represented the sorption behaviour as a function of pH, radionuclide concentration and ionic strength (only a very small dependence on the electrolyte concentration is pre-

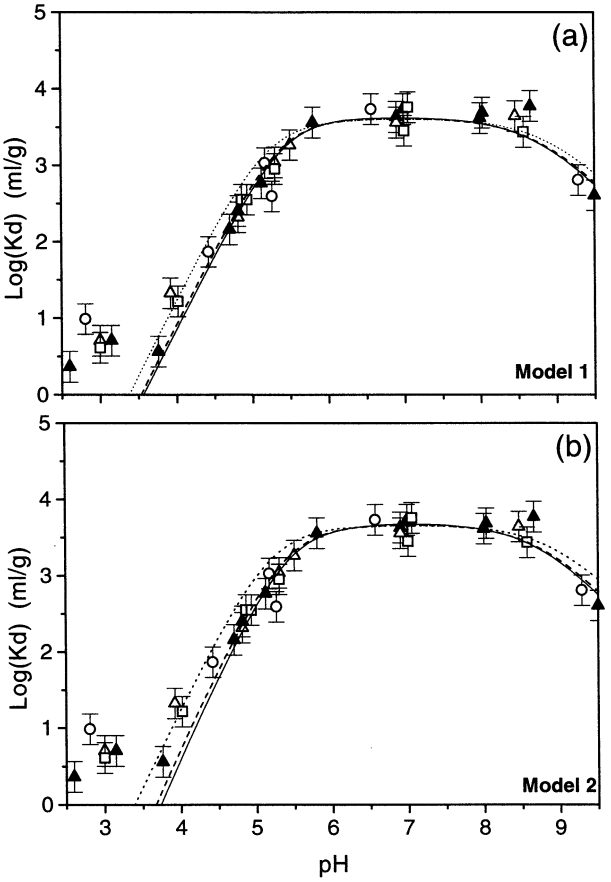

Fig. 8. Sorption edge at different ionic strengths, data expressed as log(*Kd*): (▲) $I = 0.1$ mol/L, 1 d; (△) $I = 0.1$ mol/L, 4 h; (□) $I = 0.2$ mol/L, 4 h; (○) $I = 1 \cdot 10^{-3}$ mol/L, 4 h. Modelling of the data with (a) Model 1 and (b) Model 2; (—) $I = 0.2$ mol/L; (- - -) $I = 0.1$ mol/L; (. . ..) $I = 1 \cdot 10^{-3}$ mol/L.

dicted) quite satisfactorily. The mayor discrepancy between the model and the experimental data is seen at pH < 3 and it might be caused by the partial reduction and precipitation of uranyl, which is favoured at very low pH.

The possibility of the formation of a binuclear bidentate complex (Eqn. 8) was also investigated. Only the following reaction is needed for a satisfactory fit of the experimental data (Model 2):

$$2\text{SOH} + \text{UO}_2^{2+} \Leftrightarrow (\text{SO})_2\text{UO}_2 + 2\text{H}^+ \qquad \beta_c^1$$

The parameters used to fit the experimental curves with Model 2 are summarised in Table 1. The theoretical curves of uranium sorption onto magnetite calculated with the above-mentioned parameters for the three ionic strengths shown superimposed to the experimental points in Figure 8b (sorption edges) and Figure 6 (sorption isotherm, dotted lines).

As the previous one, this model represented the sorption behaviour as a function of pH, radionuclide concentration and ionic strength quite satisfactorily. A comparison between the two models in the sorption edges obtained at $I = 1 \cdot 10^{-1}$ mol/L, is shown in Figure 5 (Model 1, continuous line and Model 2 dotted line). Both models fits the uranium inner sphere

Table A1. Sorption data (from Figure 5).

$I = 1 \cdot 10^{-3}$ mol/L; 4 h		$I = 1 \cdot 10^{-1}$ mol/L; 4 h		$I = 1 \cdot 10^{-1}$ mol/L; 1 d		$I = 2 \cdot 10^{-2}$ mol/L; 4h	
pH	U_{ads} %	pH	U_{ads} %	pH	U_{ads} %	pH	U_{ads} %
2.81	1.90	3.00	1.00	2.60	0.46	3.00	0.81
4.42	12.80	3.92	4.05	3.15	1.00	4.02	3.19
5.26	43.89	4.81	29.35	3.76	0.72	4.86	41.47
5.17	68.13	4.81	29.35	4.70	22.37	4.93	41.47
6.57	91.53	5.30	68.61	4.81	33.39	5.3	64.15
9.29	56.17	5.50	78.62	5.12	53.76	7.00	85.01
		6.90	87.85	5.80	87.82	7.05	91.96
		8.46	89.78	6.90	89.54	8.57	84.52
				6.99	91.53		
				8.00	89.20		
				8.03	90.68		
				8.66	92.19		
				9.50	44.61		

Table A2. Sorption data (from Figure 6).

Log U_{eq} (mol/L)	Log U_{ads} (mol/g)
–8.8283	–8.1191
–8.5284	–7.8635
–8.0520	–7.3366
–7.9094	–7.4410
–7.6850	–6.9980
–7.5418	–7.0845
–7.4620	–6.7980
–7.1210	–6.5050
–7.0540	–6.3020
–6.7590	–6.1140
–6.1950	–5.6450
–6.0583	–5.4049
–5.6410	–4.9550
–5.5701	–5.3093
–5.3530	–5.2390
–4.6800	

complexation equally well and they also account for the decrease in sorption observed at pH > 9. The major difference between the models is observed in the sorption isotherms at higher uranium loadings. To conclude unambiguously if the models have a general validity, some additional experiments are needed, in particular, it should be very useful to evaluate the dependence of sorption on the solid to liquid ratio. This point is being investigated. In addition, sorption experiments using a synthetic water simulating the bentonite porewater are also ongoing.

4. CONCLUSIONS

The physico-chemical properties (microstructure, surface area, surface charge) of colloidal magnetite and its stability were analysed in detail before the sorption experiments. Due to the fact that magnetite tends to dissolve in a non-negligible way at acid pH, titration experiments had to be conducted with the "fast titration" technique. Also, sorption experiments were carried out with contact times <1 d, to ensure the sorption equi-

librium and minimise both solid dissolution and possible redox effects that would have biased the experimental results. The experimental data shown in Figures 5 and 6 are given in Tables A1 and A2 respectively.

The sorption of U^{VI} onto colloidal magnetite in anoxic conditions was independent on the electrolyte concentration, indicating the formation of inner sphere complexes. Sorption isotherms showed a Langmuir-type behaviour. Sorption data were fitted, using a very simple approach, with a diffuse double layer model considering only one type of surface site. Two models were applied to fit the sorption data: the first one involving two different monodentate complexes, and the second one involving a single bidentate complex. A very good fit of both models to the uranyl sorption data in the entire range of experimental conditions investigated was found. To conclude unambiguously which is the best model to be applied, the dependence of sorption on the solid to liquid ratio should be evaluated.

Acknowledgments—This work has been partially supported by the E. C. under the contract FIKW-CT-2000-00035 (ACTAF project) and in the frame of the CIEMAT-ENRESA association. A. Yllera is thanked for his help in the synthesis of magnetite, C. Maffiotte and J.M Duran for the XPS and BET measurements, respectively. Finally, the authors wish to thank Dr. J. D. Rimstidt, Dr. J. van der Lee and an anonymous reviewer for their valuable comments on the manuscript.

Associate editor: J. D. Rimstidt

REFERENCES

Blesa M. A., Figliola N. M, Maroto A. J. G., and Regazzoni A. E. (1984) The influence of temperature on the interface magnetite-aqueous electrolyte solution. *J. Colloid Interface Sci.* **101**(2), 410–418.

Chapman N. A. and McKinley I. G. (1987) *The Geological Disposal of Nuclear Waste*. Wiley-Interscience, New York.

Cornell R. M. and Schwertmann U. (1996) *The Iron Oxides*. VCH, New York.

Dzombak D. A. and Morel F. M. (1990) *Surface Complexation Modelling*. John Wiley, New York.

El-Aamrani F., Casas I., De Pablo J., Duro L., Grivé M., and Bruno J. (2000) Experimental and modeling study of the interaction between U(VI) and magnetite. *J. Conf. Abstr.* **5,** 2–378.

Gdowski G. E. and Estill J. C. (1996) The effect of water vapor on the steel at 65°C. *Mat. Res. Soc. Symp. Proc.* **412,** 533–535.

Grambow B., Smailos E., Geckeis H., Müller R., and Hentschel H. (1996) Sorption and reduction of U(VI) on iron corrosion products under reducing saline conditions. *Radiochim. Acta* **74,** 149–154.

Grenthe I. (1992) *Chemical Thermodynamics of Uranium*. Elsevier, New York.

Hoch R., Honda A., Porter F. M., Sharland S. M., and Taniguchi N. (1997) Development of mathematical models for long-term prediction of corrosion behaviour of carbon steel overpacks for radioactive waste disposal. *Mat. Res. Soc. Symp. Proc.* **465,** 683–690.

Hsi C. D. and Langmuir D. (1985) Adsorption of uranyl onto ferric oxydroxides: Application of the surface complexation binding model. *Geochim. Cosmochim. Acta* **48,** 1931–1941.

Huang C. P. and Stumm W. (1973) Specific adsorption of cations on hydrous α-Al_2O_3. *J. Colloid Interface Sci.* **22,** 231–259.

Inagaki Y., Ogata A., Furuya H., Idemitsu K., Banba T., and Maeda T. (1996) Effects of redox condition on waste glass corrosion in the presence of magnetite. *Mat. Res. Soc. Symp. Proc.* **412,** 257–264.

Marmier N., Delisee A., and Fromage F. (1999) Surface complexation modelling of Y(III), Ni(II) and Cs(I) sorption onto magnetite. *J. Colloid Interface Sci.* **211,** 54–60.

Missana C., Maffiotte C., and Gutierrez M. G. (2003) Surface reaction kinetics between nanocrystalline magnetite and uranyl. *J. Colloid Interface Sci.* 261(1), 154–160.

Missana T., Gutierrez M. G., Fernandez C., Gil P., and Maffiotte C. (2002) Sorption of uranium onto magnetite and goethite. CIEMAT/DIAE/54610/6/02 Technical Report.

Regazzoni A. E., Urrutia G. A., Blesa M. A., and Maroto J. G. (1981) Some observation on the composition and morphology of synthetic magnetite obtained by different routes. *J. Inorg. Nucl. Chem.* **43,** 1489–1493.

Sagert N. H., Ho C. H., and Miller N. H. (1989) The adsorption of U(VI) onto a magnetic sol. *J. Colloid Interface Sci.* **130,** *1,* 283–287.

Sandino A, and Bruno J. (1992) The solubility of (VO2)3(PO4)2·4H20 and the formation of U(VI) phosphate complexes: Their influence in uranium speciation in natural waters. *Geochim. Cosmochim. Acta* **56,** 4135–4146.

Schwertmann U. and Cornell R. M. (1996) *Iron Oxides in Laboratory*. VCH, New York.

Shen J., Ebner A. D., and Ritter J. A. (1999) Point of zero charge and intrinsic equilibrium constant of silica-magnetite composite oxides. *J. Colloid Interface Sci.* **214,** 333–343.

Shultess C. P. and Sparks D. L. (1986) Backtitration technique for proton isotherm modeling of oxide surfaces. *Soil Sci. Soc. Am. J.* **50,** 1406–1411.

Silva R. J (1992) Mechanisms for the retardation of U(VI) migration. *Mat. Res. Soc. Symp. Proc.* **257,** 323–330.

Stumm W., Huang C. P., and Jenkins J. R. (1970) Specific chemical interactions affecting the stability of dispersed systems. *Croat. Chem. Acta* **42,** 223–244.

Tewari P. H. and McLean A. W. (1972) Temperature dependence of point of zero charge of alumina and magnetite. *J. Colloid Interface Sci.* **40**(2), 267–272.

van der Lee J. and De Windt L. (1999) CHESS tutorial and cookbook. Technical Report LHM/RD/99/05.

Vayssieres L., Chaneac C., Tronc E., and Jolivet J. P. (1998) Size tailoring of magnetite particles formed by aqueous precipitation: An example of thermodynamic stability of nanometric oxides particles. *J. Colloid Interface Sci.* **205,** 205–212.

Venkataramani B. and Gupta A. R. (1991) Effect of anions on the sorption of uranyl ions on hydrous oxides: Application of the surface hydrolysis model. *Colloids Surf.* **53,** 1–19.

Waite T. D., Davis J. A., Payne T. E., Waychunas G. A., and Xu N. (1994) Uranium (VI) adsorption to ferrihydrite: Application of a surface complexation model. *Geochim. Cosmochim. Acta* **58,** 5465–5478.

Wesolowski D. J., Machchesky M. L., Palmer D. A., and Anovitz L. M. (2000) Magnetite surface charge studies to 290°C from in situ pH titrations. *Chem. Geol.* **167,** 193–229.